ELSEVIER

Surface and Coatings Technology 146–147 (2001) 140–146

SURFACE & COATINGS TECHNOLOGY

www.elsevier.com/locate/surfcoat

Characterization of commercial EB-PVD TBC systems with CVD (Ni,Pt)Al bond coatings

J.A. Haynes*, M.J. Lance, B.A. Pint, I.G. Wright

Metals & Ceramics Division, Oak Ridge National Laboratory, P.O. Box 2008, Oak Ridge, TN 37831-6063, USA

Abstract

Failure of electron-beam physical vapor deposition (EB-PVD) thermal barrier coatings (TBCs) with aluminide bond coats is strongly influenced by bond coat oxidation behavior. This study investigated oxide (Al_2O_3) formation during EB-PVD processing of TBCs with (Ni,Pt)Al bond coats. The effects of substrate composition, coating impurities and bond-coat grit-blasting on the oxide phases, residual stress and microstructure were evaluated. As-deposited, high-purity commercial bond coats contained high concentrations of sulfur and other impurities at their surfaces. Numerous small voids formed at the oxide–metal interface when as-deposited bond coats were oxidized during EB-PVD processing. Grit-blasting of (Ni,Pt)Al had a significant impact, since the formation of α-Al_2O_3 during EB-PVD processing was significantly enhanced and voids did not form beneath the scale. Preliminary cyclic oxidation testing suggested an influence of superalloy sulfur content on TBC durability. © 2001 Elsevier Science B.V. All rights reserved.

Keywords: Electron-beam physical vapor deposition (EB-PVD); Thermal barrier coating (TBC); Aluminide bond coat

1. Introduction

Thermal barrier coating (TBC) systems reduce the operating temperature of hot-section superalloy hardware in gas turbine engines [1]. A typical TBC consists of an oxidation-resistant metallic bond coat overlaid with a thermally insulating ceramic top coat of Y_2O_3–ZrO_2 (YSZ). The bond coat oxidizes to form a protective scale of Al_2O_3 during deposition of the top coat, and during subsequent exposure in service. Spallation of the YSZ top coat is often associated with eventual failure of the underlying Al_2O_3 scale [2,3]. Thus, one clear path to improved TBC performance is design of bond coats with optimized Al_2O_3 adherence.

The growth and adherence characteristics of Al_2O_3 scales are not completely understood and are sensitive to a number of factors, including oxide phase content, bond coat surface finish, and bond coat and substrate composition. For example, formation of α-Al_2O_3 can be accelerated by surface roughening of aluminide bond coats [4,5]. Furthermore, appropriate surface finishing (e.g. grit-blasting) of aluminide bond coats apparently prevents premature TBC spallation [1]. Reduction of substrate S impurities to <1.0 ppm drastically improves scale adherence to alumina-forming alloys [6,7] and coatings [2,8,9]. Alternatively, additions of a precious metal, such as Pt [8,10–13], or trace amounts of a reactive element, such as Y, Hf or Zr, can dramatically improve scale adherence [14]. Both S and reactive elements can diffuse from the superalloy through the bond coat to influence oxide growth and adherence [13]. This paper describes preliminary efforts to systematically study the effects of superalloy substrate composition and bond coat surface finish on Al_2O_3 phase formation, residual stress and microstructure within commercial EB-PVD TBCs with (Ni,Pt)Al bond coatings.

2. Experimental

2.1. Specimen fabrication

Three variations of René N5 superalloy were cast as single-crystal rods (Howmet Research Corporation,

* Corresponding author. Tel.: +1-865-576-2894; fax: +1-865-574-6918.

E-mail address: haynes@ornl.gov (J.A. Haynes).

0257-8972/01/$ - see front matter © 2001 Elsevier Science B.V. All rights reserved.
PII: S0257-8972(01)01483-9

Table 1
Types of coated specimens

Specimen type	Coating source	Substrate type	Bond coat surface	YSZ top coat
UHP	Laboratory	HS	Not grit-blasted	No
B	Commercial	HS, LS, Y	Not grit-blasted	No
BG	Commercial	HS, LS, Y	Grit-blasted	No
C	Commercial	HS, LS, Y	Grit-blasted	Yes
D	Commercial	HS, LS, Y	Grit-blasted	Yes
E	Commercial	HS, LS, Y	Not grit-blasted	Yes

A hole was drilled through type B, D and E specimens for hanging during oxidation testing. Type C specimens did not have a through-hole.

Whitehall, MI). The three alloys were as follows: (1) high-sulfur (alloy HS) with 2–3 ppm S, (2) lower-sulfur (alloy LS) which was melt-desulfurized to <1.0 ppm S; and (3) Y-containing (alloy Y) with 2–3 ppm S and 100 ppm Y. Superalloy compositions were measured by inductively coupled plasma (ICP) analysis. Sulfur was measured by glow-discharge mass spectroscopy (GDMS).

Discs (16.5 mm in diameter $\times$1.6 mm) of each type superalloy were electroplated with $\sim$7 μm Pt (Howmet Research Corporation, Whitehall, MI). All substrates were Pt-plated in the same batch. Most of the Pt-plated specimens were aluminized by a commercial, high-temperature, low-activity CVD process (Howmet, MDC 150L) [15]. Other Pt-plated specimens were aluminized via a very similar process, using a laboratory-scale CVD reactor that had been designed to minimize sulfur contamination, as described elsewhere [2,8,9]. Specimens coated in the laboratory reactor will be specifically referred to as ultra-high-purity (UHP) bond coatings. There were no post-aluminizing heat treatments of either batch of bond coatings. Both processes resulted in single-phase β-(Ni,Pt)Al bond coats.

A standard procedure after aluminizing is to grit-blast the aluminide bond coat with Al_2O_3 prior to EB-PVD of the YSZ top coating. However, in order to evaluate the effects of grit-blasting, TBCs in this study were prepared both with and without grit-blasting of the bond coat surface. Selected commercial bond coatings (grit blasted and non-grit blasted) were coated with EB-PVD YSZ top coatings ($\sim$150 μm thick) on one face (Howmet). The UHP bond coats were not coated with YSZ; thus, all TBC specimens possessed a commercial bond coat. The various types of specimens are summarized in Table 1.

2.2. Coating characterization

Major, minor and trace elements in the as-deposited UHP and commercial bond coats were qualitatively measured by GDMS sputter depth-profiling. Surface and metallographic cross-sections of as-deposited bond coat and TBC specimens were characterized by field-emission gun scanning electron microscopy (FEG-SEM; Hitachi S4700, Tokyo, Japan).

The stress state and phase content of the alumina scales that formed during YSZ deposition were determined by photo-stimulated luminescence spectroscopy (PSLS) [16,17]. Measurements were made using a Dilor XY 800 Raman microprobe configured to operate as a single-stage spectrograph with an argon ion laser (Innova 308c, Coherent Inc) operating at 5145 Å with an output power of 500 mW. An attached microscope focused the incident laser to a spot size of 10–12 μm onto the TBC surface [17].

2.3. Cyclic oxidation testing

Cyclic oxidation testing was performed in a dry flow of oxygen at 1150°C in an automated furnace. Specimens hanging from Pt–Rh wires were inserted into a hot furnace, remained at temperature for 60 min, and were then removed and allowed to cool for 10 min between cycles to ambient temperature ($\sim$30°C).

3. Results

3.1. Superalloy and bond coat compositions

The average levels (by ICP) of the major elements in the three batches of superalloy were very similar, as shown in Table 2. Note that there was no reduction in Hf or C in the LS alloy due to the melt de-sulfurization process, as can occur during H_2 desulfurizing.

The values measured for sulfur in the HS, Y and LS alloys were 2.5 ± 0.2, 2.0 ± 0.2 and 0.9 ± 0.4 ppm, respectively, by GDMS (Table 2). The differences measured in sulfur and yttrium correlated very well with the relative oxidation behavior of the superalloys, since the LS and Y alloys (without coatings) displayed superior

Table 2
Compositions of Rene N5 substrate batches

Element	Superalloy composition (wt.%)		
	High-S	High-S+Y	Low-S
Ni	63.4	63.4	63.7
Cr	7.1	7.0	6.9
Co	7.3	7.0	7.1
Al	6.3	6.2	6.2
Ta	6.5	6.5	6.6
W	4.9	4.8	4.8
Re	2.9	2.8	2.9
Mo	1.7	1.7	1.7
Hf (ppm)	1500	1400	1600
C (ppm)	300	500	500
Zr (ppm)	100	100	100
Y (ppm)	<3	<3	100
S[a] (ppm)	2.5	2.0	0.9

[a] S measured by GDMS, all other elements by ICP.

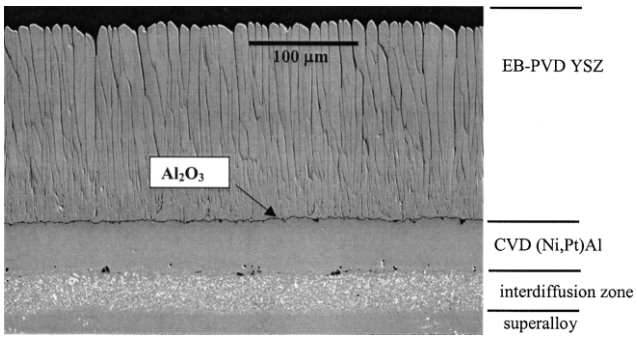

Fig. 1. SEM images of a cross-section of an as-deposited TBC with a grit-blasted CVD (Ni,Pt)Al bond coat. The alumina scale is the thin dark-contrast layer along the YSZ–(Ni,Pt)Al interface.

scale adherence to that of the HS alloy during cyclic oxidation testing at 1100 and 1150°C.

A typical cross-sectional SEM image of an as-deposited TBC is shown in Fig. 1. The (Ni,Pt)Al bond coats were ~42 μm thick. The near-surface composition of the commercial CVD (Ni,Pt)Al, as measured by electron microprobe of a cross-section (in wt.%), was 55.4 Ni (47.8 at.%), 22.8 Al (42.8 at.%), 4.7 Co, 13.1 Pt (3.4 at.%) and 1.9 Cr.

3.2. GDMS sputter profiling of coatings

Major and trace element concentration profiles in an as-received commercial bond coating (specimen BHS1) and a UHP laboratory bond coating (UHP1) on the HS substrates were qualitatively determined by GDMS sputter depth-profiling (Fig. 2a–d). The accuracy of the GDMS sputter profile data should be viewed with some caution, since resolution is influenced by the shape of the sputter crater, as well as by re-deposited material [2,18]. The experiments were configured to maximize the resolution of sulfur measurements in the near-surface region.

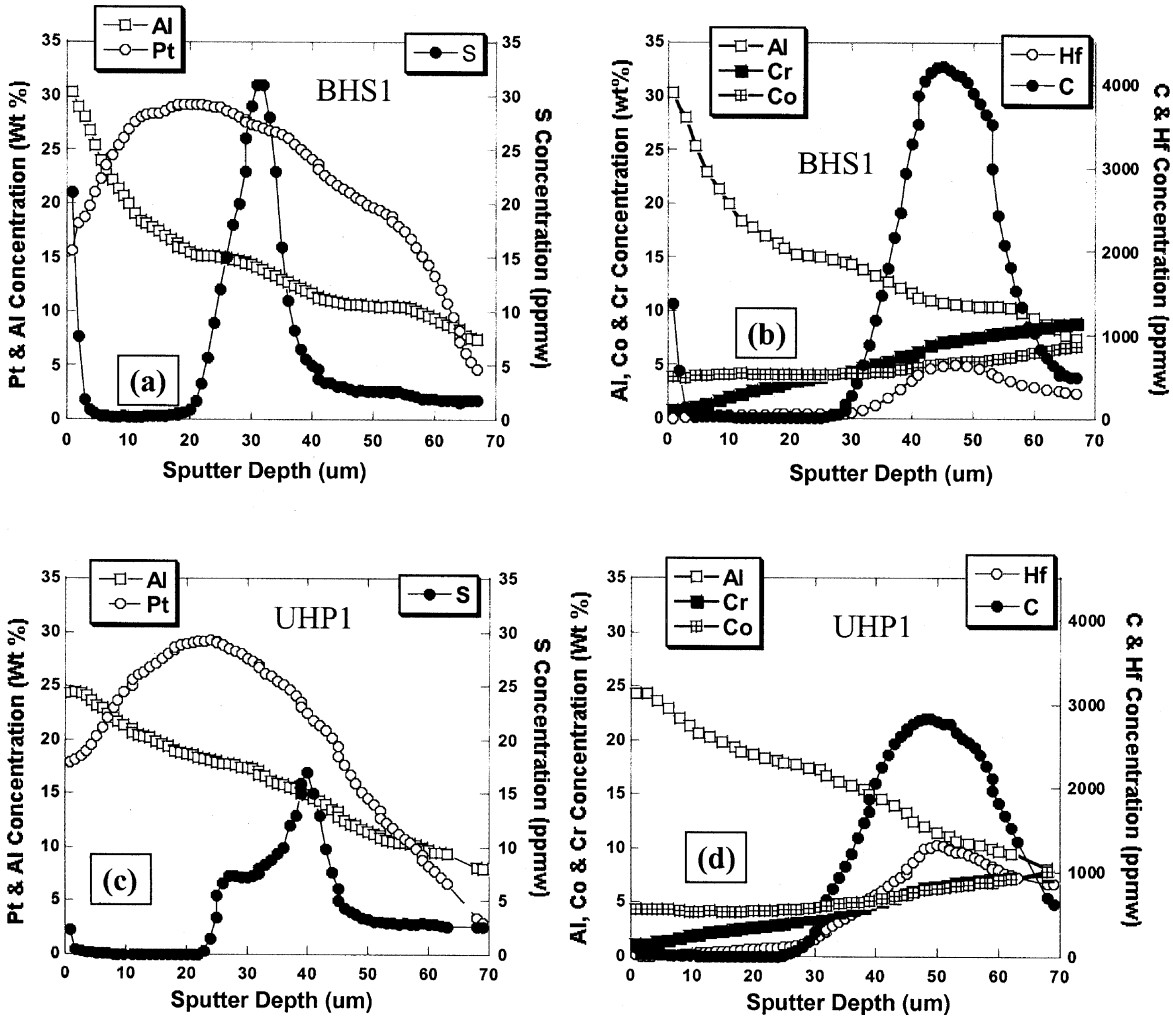

Fig. 2. GDMS sputter depth profiles across as-deposited CVD (Ni,Pt)Al bond coats on identical HS substrates. Both specimens were Pt-plated in the same bath. (a,b) High-purity commercial CVD bond coat (BHS1); and (b,d) laboratory-scale ultra-high-purity bond coat.

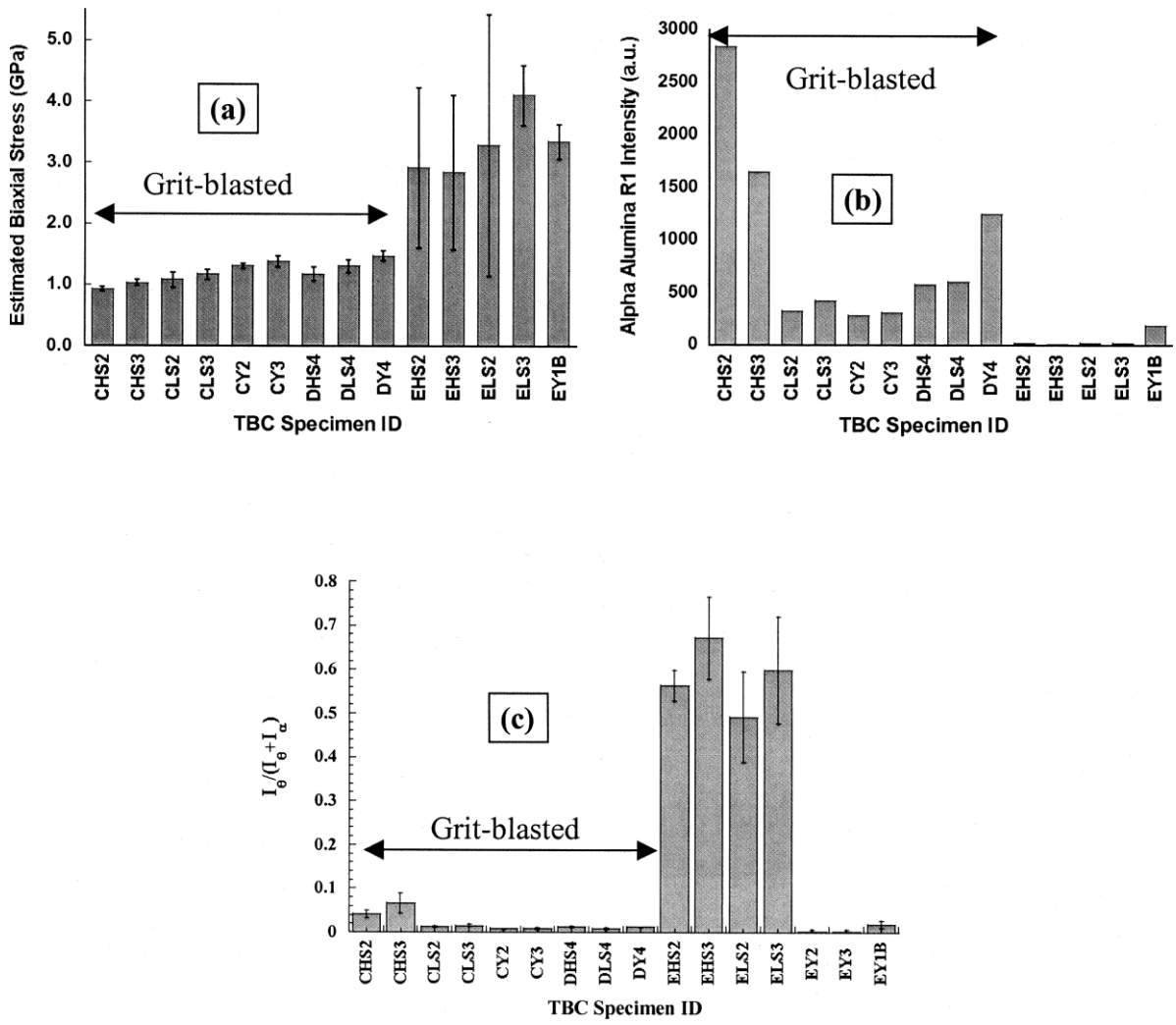

Fig. 3. PSLS measurements on as-deposited EB-PVD TBCs with varying substrate compositions and bond coat surface conditions. (a) Biaxial stress in α-Al_2O_3; (b) intensity of α-Al_2O_3 signal; and (c) ratio of θ-Al_2O_3 to α-Al_2O_3 intensity.

Impurity (C and S) concentrations at the surface of BHS1 (Fig. 2a,b) were much higher than those on UHP1 (Fig. 2c,d), although the sub-surface region of both coatings (Fig. 2a,b) was very pure (e.g. <0.5 ppm S). The S concentration at the surface of BHS1 ($\sim$21 ppm) was approximately nine-fold that of UHP1 ($\sim$2.3 ppm), and the C concentration was 14-fold that of UHP1. Both coatings exhibited large internal impurity peaks (Fig. 2a,c) near the original superalloy surface due to contamination during Pt plating [9].

The C concentration in both coatings peaked at a depth of $\sim$10 μm below the coating–superalloy interface. These C peaks also coincided with the peak concentrations of Zr and Hf, likely due to the formation of carbides in the interdiffusion zone. Other trace impurities (N, S, P and Cl) mimicked S and segregated at the surface and interface of both coatings, albeit at much higher concentrations in BHS1 than in UHP1. The amounts of O, Na, and Ca segregated at the surface were also much higher for BHS1, but the concentrations at the coating–substrate interface were similar for both coatings.

3.3. Oxide residual stress

Results of the PSLS analyses of the alumina scales beneath as-deposited TBCs are shown in Fig. 3a–c. Both α- and θ-alumina were detected beneath all TBCs. There was a significant influence of grit-blasting on the relative amounts of each phase and on α-Al_2O_3 residual stress. Oxide scale biaxial stresses were higher on Type E TBCs with smooth bond coat surfaces (Fig. 3a). The mean compressive stress values were measurably lower on Types C and D TBCs with grit-blasted bond coats (Fig. 3a), as expected, due to out-of-plane tensile stresses introduced by surface perturbations.

Fig. 3b compares the intensity (in arbitrary units, a.u.) of the α-Al_2O_3 signals. Note that the α-Al_2O_3

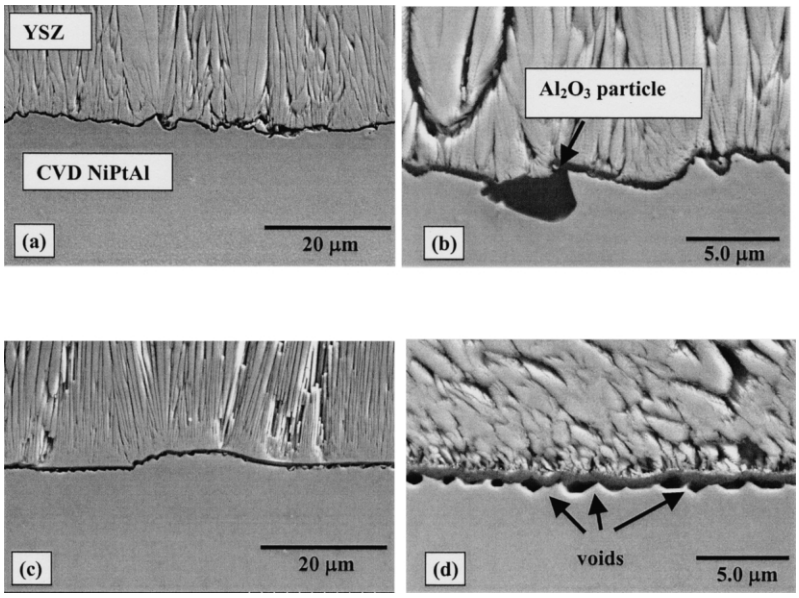

Fig. 4. SEM images of cross-sections of the interfacial region of as-deposited TBCs. (a) Grit-blasted interface; (b) higher magnification of oxide scale and grit-blast particle (arrow) on bond coat; (c) interface of a TBC that was not grit-blasted, with a grain-boundary ridge visible; and (d) voids (arrows) observed beneath the oxide scales on non-grit-blasted surfaces.

intensity is much higher on grit-blasted bond coats. Fig. 3c compares the ratio of θ-Al_2O_3 to α-Al_2O_3 intensity. The relative intensity of θ-Al_2O_3 was very low on grit-blasted specimens. Higher θ-Al_2O_3 intensity was measured on E-series TBCs (Table 1) with smooth bond coat surfaces, with the exception of EY1B (Fig. 3b). Specimen EY1B was coated in a different EB-PVD batch than the other E-series specimens, which suggests that differences in oxide phase content can be strongly influenced by EB-PVD process variables, such as local temperature.

3.4. Influence of grit-blasting

The bond coat–top coat interface of an as-deposited Type D TBC (grit-blasted bond coat) is shown in Fig. 4a,b. No voids were observed beneath the oxide scales that formed during EB-PVD of YSZ onto grit-blasted (Ni,Pt)Al surfaces.

Oxide scale growth was dramatically different on Type E TBCs with as-deposited (not grit-blasted) bond coat surfaces (Fig. 4c,d). Numerous small voids (0.2–1.2 μm in diameter) were observed at the oxide–metal interface (Fig. 4d), as recently reported [19]. In fact, voids were observed on all as-deposited (Ni,Pt)Al surfaces (regardless of superalloy substrate composition), even the non-grit-blasted edges of the Type D TBCs. Higher magnification images of the oxide–metal interfaces are compared in Fig. 5a,b. These differences on as-deposited and grit-blasted surfaces, even on the same specimen, suggest that modifications in void formation behavior were not the result of EB-PVD processing variations.

3.5. Thermal cycle testing

Cyclic oxidation testing of bare bond coats and TBCs on the three types of substrate was conducted at 1150°C.

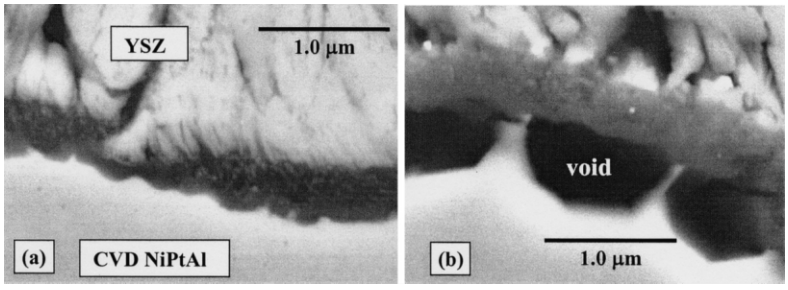

Fig. 5. SEM images of oxide scales within as-deposited TBCs. (a) Oxide scale on a grit-blasted bond coat. (b) Oxide on a smooth bond coat, with faceted, hemispherical voids beneath the α-Al_2O_3 scale.

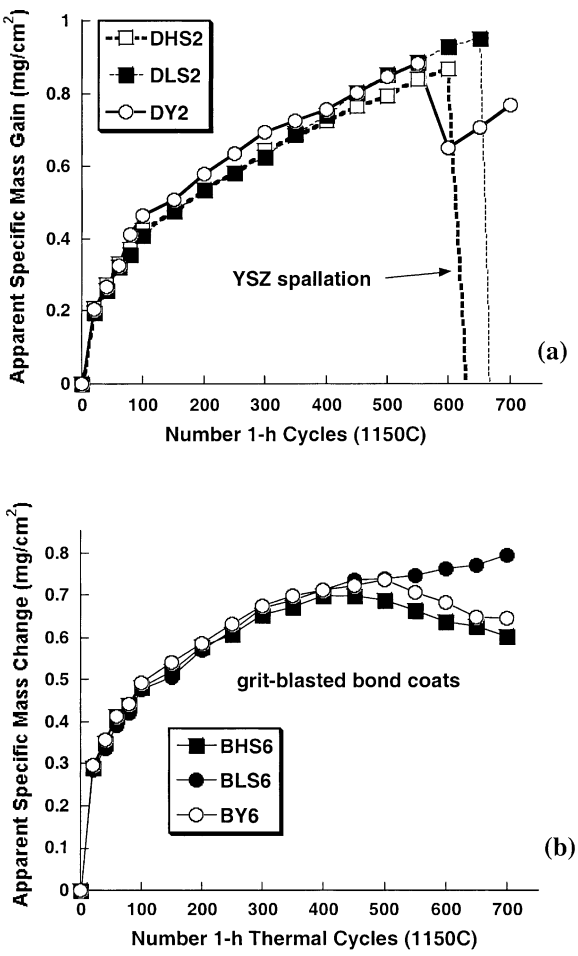

Fig. 6. Plots of the 1150°C cyclic oxidation behavior of coatings on the three types of superalloy. (a) grit-blasted bare CVD (Ni,Pt)Al bond coats; and (b) EB-PVD TBCs with grit-blasted CVD (Ni,Pt)Al bond coats.

Three bare bond coat specimens, each grit-blasted on one surface (Type BG, Table 1), exhibited near-identical rates of mass gain until approximately 500 cycles (Fig. 6a). Bond coats on the HS and Y type superalloys began to exhibit Al_2O_3 scale spallation at 500 and 550 cycles, respectively. In contrast, there was little evidence of mass loss from the bond coat on the melt desulfurized (LS) superalloy after 700 cycles. For YSZ-coated specimens (with grit-blasted bond coats, Type D, Table 1), the YSZ spalled first on the Y alloy between 550 and 600 cycles (Fig. 6b). The YSZ on the HS alloy spalled between 600 and 650 cycles, whereas the YSZ on the LS alloy spalled between 650 and 700 cycles. The rate of mass gain for the TBCs appeared to be identical to that of the bare bond coats, and the YSZ on all three TBCs spalled from the center outward. As in the case of the Al_2O_3 scales on the bare bond coats, there appeared to be a trend of longer TBC lifetimes on the superalloy with reduced sulfur. Apparently, Y in the superalloy was not effective in improving bond-coat oxidation performance. Detailed characterization and subsequent testing of larger coating populations will provide a more conclusive indication of whether superalloy composition and grit-blasting influence TBC life.

4. Discussion

The results in Fig. 3c suggest that bond-coat grit-blasting either suppresses θ-Al_2O_3 nucleation or triggers more rapid transformation to or nucleation of α-Al_2O_3 during EB-PVD processing at $\sim$1000°C. These results demonstrate that scale growth during fabrication of actual TBCs on grit-blasted aluminide bond coats is similar to that of bare bond coat surfaces exposed to furnace oxidation [4,5]. Grit-blasting removes surface impurities, such as C and S (Fig. 2a,b), which might also influence oxide nucleation and transformation behavior.

The results of this study also show that grit-blasting eliminates the detrimental process of interfacial void growth during EB-PVD processing (Figs. 4 and 5). Previous studies have shown that although the rate of void growth on simple aluminide coatings increased as S impurities increased [13], Pt-modified aluminides were very resistant to void growth and were much less sensitive to the presence of S impurities [12,13]. However, subsequent work has shown that voids will form on (Ni,Pt)Al if coating or substrate sulfur levels are high enough [19]. It appears that the 21 ppm S detected at the surface of the (Ni,Pt)Al bond coats in this study (Fig. 2a) exceeded some critical impurity threshold for void formation on (Ni,Pt)Al. Thus, it is likely that the elimination of void growth in the grit-blasted specimens was related to removal of the sulfur-contaminated zone at the surface of the coating (Fig. 2a). This impurity-related conclusion is supported by the observation that lightly polishing the surface of as-deposited CVD (Ni,Pt)Al bond coats (which would remove surface sulfur, but should not contribute to enhanced α-Al_2O_3 formation) prior to TBC deposition dramatically increases EB-PVD TBC life [3].

Volume reductions associated with the $\theta \rightarrow \alpha$-$Al_2O_3$ transformation could also contribute to void formation. However, the large size of the voids, relative to scale thickness, suggests that more than just a phase transformation was involved in void growth. Void growth on grit-blasted surfaces could also be reduced by the accelerated transformation to α-Al_2O_3, since θ-Al_2O_3 (which primarily grows by outward transport of Al) would have a greater tendency to leave Kirkendall voids at the oxide–metal interface. However, at this time there is insufficient information to determine the dominant driving force(s) behind the differences observed in void growth.

Finally, it can be concluded that void growth of the type shown in Figs. 4 and 5 is a contributor to premature

failure of TBCs when aluminide bond coat surfaces are not 'properly' surface-finished. Thus, it can be concluded that in addition to more rapid nucleation of α-Al_2O_3, one of the major benefits of grit-blasting is the elimination of void growth during EB-PVD processing, which reduces the probability of premature YSZ spallation. However, with regard to ultimate TBC durability, it may actually be more beneficial to develop processing or finishing methods that do not require roughening of the bond coat surface to either remove sulfur or nucleate the desired Al_2O_3 phase, since it has been shown that very light polishing of CVD (Ni,Pt)Al surfaces, combined with controlled heat treatments, can also provide significant improvements in TBC durability [3].

5. Summary

As-deposited commercial CVD (Ni,Pt)Al bond coats exhibited very high impurity (S, C and N) concentrations at their surfaces, although the bulk coatings were very pure. As-deposited (Ni,Pt)Al surfaces formed copious amounts of very fine voids beneath the Al_2O_3 scale during EB-PVD processing. Grit-blasting of the bond coat eliminated void growth, possibly due to removal of S, and increased the rate of α-Al_2O_3 formation. Preliminary cyclic oxidation testing (1150°C) of TBCs suggested slight increases in spallation life on desulfurized superalloys.

Acknowledgements

The authors thank B. Pachman, B. Warnes and K. Murphy of Howmet Research Corporation for superalloy casting and coating fabrication. Thanks are extended to T. Geer for metallography, L.W. Walker for microprobe analysis, M.P. Brady and P.F. Tortorelli, all of ORNL, for helpful reviews. Research sponsored by the US Department of Energy, Office of Power Technologies, Advanced Turbine Systems Program under Contract DE-AC05-00OR22725 with UT-Battelle, LLC.

References

[1] D.V. Rigney, R. Viguie, D.J. Wortman, D.W. Skelly, J. Therm. Spray Technol. 6 (2) (1997) 167.
[2] W.Y. Lee, Y. Zhang, I.G. Wright, B.A. Pint, P.K. Liaw, Metall. Trans. A 29 (1998) 833.
[3] M. Gell, E. Jordan, K. Vaidyanathan et al., Surf. Coat. Technol. 120-121 (1999) 53.
[4] V.K. Tolpygo, D.R. Clarke, Mater. High Temp. 17 (1) (2000) 59.
[5] D. Monceau, K. Bouhanek, R. Peraldi, A Malie, B. Pieraggi, J. Mater. Res. 15 (3) (2000) 665.
[6] J.G. Smeggil, A.W. Funkenbusch, N.S. Bornstein, Metall. Trans. A 17 (1986) 923.
[7] J.L. Smialek, Metall. Trans. A 18 (1987) 164.
[8] J.A. Haynes, Y. Zhang, W.Y. Lee, B.A. Pint, I.G. Wright, K.M. Cooley, in: J.M. Hampikian, N.B. Dahotre (Eds.), Elevated Temperature Coatings: Science and Technology III, TMS, Warrendale, PA, 1998, p. 185.
[9] Y. Zhang, W.Y. Lee, J.A. Haynes et al., Metall. Trans. A 30 (1999) 2679.
[10] E.J. Felten, F.S. Pettit, Oxid. Met. 10 (1976) 189.
[11] B.A. Pint, I.G. Wright, W.Y. Lee, Y. Zhang, K. Prüßner, K.B. Alexander, Mater. Sci. Eng. A 245 (1998) 201.
[12] Y. Zhang, J.A. Haynes, W.Y. Lee, et al., Effects of Pt incorporation on the isothermal oxidation behavior of CVD aluminide coatings, Metall. Trans. A, in press.
[13] J.A. Haynes, K.L. More, B.A. Pint, I.G. Wright, K. Cooley, Y. Zhang, in: R. Streiff, R.C. Krutenat, M. Caillet, I.G. Wright (Eds.), High-Temperature Corrosion and Protection of Materials, 5, 2001, p. 679.
[14] B.A. Pint, Oxid. Met. 45 (1/2) (1996) 1.
[15] W.C. Basta, D.C. Punola, B.M. Warnes, US Patent 5 658 614, 1997.
[16] R.J. Christensen, D.M. Lipkin, D.R. Clarke, K. Murhpy, Appl. Phys. Lett. 69 (24) (1996) 3754.
[17] M.J. Lance, J.A. Haynes, W.R. Cannon, M.K. Ferber, in: C.H. Schilling, J.N. Gray (Eds.), Ceramic Transactions: Non-Destructive Evaluation of Ceramics, 89, American Ceramic Society, Westerville, OH, 1998, p. 229.
[18] I.T. Spitsberg, K. Putyera, Surf. Coat. Technol. 139 (1) (2001) 35.
[19] J.A. Haynes, Scr. Mater. 44 (7) (2001) 1147–1152.